



Calibration of residual polarization in light source for broadband rotating polarizer spectroscopic ellipsometer

Ming Gong^a, Honggang Gu^{b,c,*}, Chao Chen^b, Jun Chen^d, Weiqi Li^d, Chuanwei Zhang^{b,c}, Shiyuan Liu^{b,c}

^a School of Optical and Electronic Information, Huazhong University of Science and Technology, Wuhan, Hubei, 430074, China

^b State Key Laboratory of Digital Manufacturing Equipment and Technology, Huazhong University of Science & Technology, Wuhan, 430074, China

^c Optics Valley Laboratory, Hubei, 430074, China

^d Wuhan Eoptics Technology Co. Ltd., Wuhan, 430075, China

ARTICLE INFO

Keywords:

Spectroscopic ellipsometry
Rotating polarizer
Residual polarization
Calibration

ABSTRACT

The rotating polarizer spectroscopic ellipsometer (RPSE) has many advantages, such as simple optical configuration and broadband achromatism. However, the final performances of the RPSE will be significantly degraded by the residual polarization in light source. Therefore, we propose a three-step method to calibrate and correct the residual polarization in the light source of the RPSE. We establish a system model to describe the RPSE system considering the residual polarization in light source, in which two parameters b and c in the Stokes vectors of the light source are introduced to characterize the residual polarization. The three-step method including two global calibrations and one wavelength by wavelength calibration aims to obtain the accurate systemic parameters and b , c of the RPSE. And we develop an RPSE instrument to verify the three-step calibration method experimentally. The accuracy of corrected results considering the residual polarization is improved dramatically compared with the uncorrected results. Apart from the rotating polarizer ellipsometer, the calibration method implemented in this work is also applicable to other broadband rotating element ellipsometers.

1. Introduction

Spectroscopic ellipsometry (SE) detects and analyzes the polarized light-matter interactions by modulating and demodulating the polarization state of light. It is a nondestructive, low-cost, self-consistent and high-precision technique, and has been developed as a powerful tool for the characterization of nanomaterials, nanofilms and nanostructures in both of nanoscience and nanomanufacturing especially the semiconductor industry [1–9]. In general, spectroscopic ellipsometers can be classified into different types according to the polarization modulation principles, such as the mechanical rotation [10], electric-driving modulation [11], or spatial division of amplitude [12], etc. Among them, the rotating-element ellipsometer achieving polarization modulation by mechanical rotation is the most commonly applied type due to the unique advantages, such as easy operations in hardware implementation and data processing, ultra-wide applicable spectral range, as well as compact architecture. In the history of succession, the rotating-polarizer ellipsometer firstly appeared in 1970s, then followed by the

rotating-compensator ellipsometer [13,14]. The latter has the advantage of complete Mueller matrix measurement with a dual rotating-compensator configuration [9,15–17], and consequently is more popular for complex applications, such as depolarization [18] and optical anisotropies measurement [19,20]. Although the rotating-polarizer ellipsometer fails to achieve the complete Mueller matrix in principle, the polarizer is usually not limited by the severe dispersion in material that will significantly degrade the performance of the ellipsometer, and thus can be applied for wider spectral range. Since the simpler architecture and absence of chromatic elements, the rotating-polarizer ellipsometer can be easily extended to broadband applications covering from the ultraviolet to infrared ranges [21].

The rotating-polarizer ellipsometer has several different configurations depending on the positions of the rotating polarizer, typically including the rotating polarizer ellipsometer (RPE) with the polarizer rotating on the source arm [22–25], the rotating analyzer ellipsometer (RAE) with the analyzer rotating on the detection arm [26–31], and rotating polarizer-analyzer ellipsometer (RP AE) with both the polarizer

* Corresponding author at: Nanoscale and Optical Metrology Group, School of Mechanical Science and Engineering, Huazhong University of Science and Technology, Luoyu Road 1037, Wuhan, Hubei 430074, China.

E-mail address: hongganggu@hust.edu.cn (H. Gu).

<https://doi.org/10.1016/j.tsf.2023.139739>

Received 28 September 2022; Received in revised form 19 January 2023; Accepted 12 February 2023

Available online 15 February 2023

0040-6090/© 2023 Elsevier B.V. All rights reserved.

rotating on the source arm and analyzer rotating on the detection arm [32–37]. Each configuration has advantages and disadvantages. In detail, the RPE system is free of polarization-dependent sensitivity of the detector but suffers from the residual polarization in light source [24]. On the contrary, the RAE system avoids the residual polarization in light source but requires increased attentions to calibrate and compensate the polarization-dependent sensitivity of the detector [26]. While the RPAE may suffer both from the residual polarization of the light source and polarization-dependent sensitivity of the detector, but it can achieve more information (up to 9 elements in the upper left corner of the Mueller matrix) by synchronously rotating the polarizer and analyzer in different angular velocities [5,10]. Therefore, the calibration and correction of the residual polarization in light source and the polarization-dependent sensitivity of the detector are essential to ensure the performances of the rotating polarizer/analyzer ellipsometer.

Methods to deal with the residual polarization in light source have been discussed for a long time. S. Bertucci *et al.* [38] and A. E Naciri *et al.* [24] respectively proposed a RPE configuration by additionally introducing a fixed polarizer in front of the rotating polarizer to eliminate the residual polarization in light source. In theory, the additional fixed polarizer would generate linearly polarized light, and reduce influences of the residual polarization in light source. However, it will greatly sacrifice the light intensity which further degrades the signal-to-noise ratio and consequently the measurement precision, and also make the system architecture and calibration more complex. Another typical method is to introduce a depolarizer in front of the rotating polarizer to filter out the residual polarization to produce a completely unpolarized light source. However, the depolarizer is essentially a specifically designed retarder with different phase retardation at different areas and wavelengths, and the light passing through the depolarizer is a synthesis of random polarization state, which produces integral effect of depolarization in the spatial domain. These devices are so called “pseudo-depolarizers” [39]. Although some depolarizers have advanced performance with a degree of polarization less than 10% [40], it is still far from sufficient for this kind instruments. Therefore, the additional depolarizer fails to address the residual polarization of light source in practice. In summary of these existing methods, most of them rely on additional hardware, e.g., fixed polarizer or depolarizer, to reduce the residual polarization in light source, and rare studies deal with this issue from a software perspective, such as calibration and correction of the residual polarization by introducing additional systematic parameters in the data processing.

On the basis of the above situation and discussion, in this paper, we would like to talk about the calibration and correction of the residual polarization in light source for a broadband RPSE. Firstly, we construct a

system model for the RPSE using the Stokes-Mueller formulas by considering the residual polarization in light source. Then, we propose a so-called three-step method to *in-situ* calibrate the residual polarization in light source, and consequently correct it in the ellipsometric measurement. Finally, a broadband RPSE covering the ultra-wide spectral range of 193~1000 nm is developed to perform the experiments based on the proposed methods. Results clearly demonstrate the effectiveness and advantages of the proposed methods in calibrating and correcting the residual polarization in light source for broadband RPSE configurations.

2. Theories and methods

2.1. System model of RPSE considering residual polarization in light source

The RPSE can be optically represented by PrSA, where Pr stands for rotating polarizer, S for the sample under test and A for the fixed analyzer. Fig. 1 depicts the principle diagram of a typical RPSE system.

The Stokes vector \mathbf{S}_{out} received by the detector can be expressed in the form of Mueller matrix multiplication:

$$\mathbf{S}_{\text{out}} = [\mathbf{R}(-A_0)\mathbf{M}_A\mathbf{R}(A_0)]\mathbf{M}_S[\mathbf{R}(-P)\mathbf{M}_P\mathbf{R}(P)]\mathbf{S}_{\text{in}}, \quad (1)$$

where, \mathbf{S}_{in} is the Stokes vector of the light source, $\mathbf{R}(\bullet)$ is the Mueller matrix of coordinate rotation, \mathbf{M}_P , \mathbf{M}_A and \mathbf{M}_S are the Mueller matrixes of the polarizer, analyzer and sample respectively, and A_0 and P are the azimuth angles of the fixed analyzer and the rotating polarizer respectively. Since the polarizer is rotated continuously, we have $P = \omega t - P_0$, where ω and P_0 are the mechanical angular frequency of the rotation and the original equivalent fast axis azimuth (i.e., at the time $t = 0$) of the polarizer.

As to the RPSE, generally if we default the residual polarization in light source to be ignored, namely the Stokes vector of the light source \mathbf{S}_{in} is $[1 \ 0 \ 0 \ 0]^T$, the irradiance received by the detector can be expressed by the first element of the Stokes vector \mathbf{S}_{out} derived by expanding Eq. (1) as given by

$$I = I_0[1 + \alpha \cos 2P + \beta \sin 2P], \quad (2)$$

where, α and β are the normalized Fourier coefficients of double frequency terms, and I_0 is the DC component which is used to normalize the Fourier coefficients.

When the residual polarization in light source is taken into consideration, the Stokes vector of the light source can be given as $[1 \ b \ c \ 0]^T$, where b and c are parameters describing the residual polarization in light source. The last parameter of Stokes vector of light source are set to

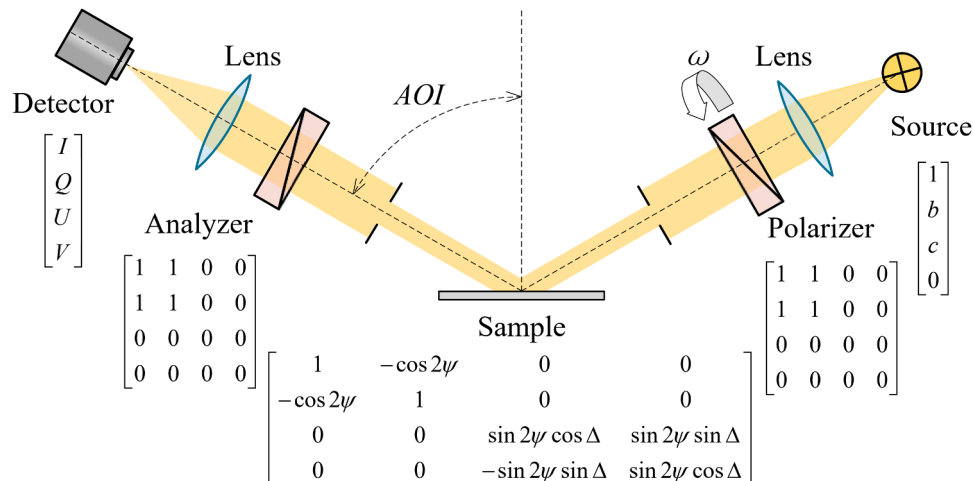


Fig. 1. Principle diagram of a typical RPSE system.

0 because it will always be eliminated in the expression of I for RPSE. And only the second parameter b and third parameter c will affect the system. Therefore, for simplicity, the Stokes vector is given in the form of $\mathbf{S}_{in} = [1, b, c, 0]^T$ in this work. In this case, the irradiance received by the detector is changed as the following expression,

$$I = I_0[1 + \alpha \cos 2P + \beta \sin 2P + \alpha' \cos 4P + \beta' \sin 4P], \quad (3)$$

where, α and β are the normalized Fourier coefficients of double frequency terms, and α' and β' are the normalized Fourier coefficients of quadruple frequency terms. These Fourier coefficients are given by

$$\alpha = \frac{b - b \cos 2\psi \cos 2A + \cos 2A - \cos 2\psi}{\alpha_0}, \quad (4)$$

$$\beta = \frac{c - c \cos 2\psi \cos 2A + \sin 2A \sin 2\psi \cos \Delta}{\alpha_0}, \quad (5)$$

$$\alpha' = \frac{0.5b(\cos 2A - \cos 2\psi)}{\alpha_0}, \quad (6)$$

$$\beta' = \frac{0.5(c \cos 2A - c \cos 2\psi + b \sin 2A \sin 2\psi \cos \Delta + c \sin 2A \sin 2\psi \cos \Delta)}{\alpha_0}, \quad (7)$$

$$\alpha_0 = 1 - \cos 2\psi \cos 2A + 0.5b(\cos 2A - \cos 2\psi). \quad (8)$$

Herein, quadruple frequency terms $\cos 4P$ and $\sin 4P$ appear when the light source contains residual polarization. And the magnitudes of Fourier coefficients α' and β' quantitate the level of the residual polarization in light source.

2.2. Three-step method to calibrate the residual polarization in light source

The residual polarization is related to the type of light source used by the instrument. Let's suppose lamp A and lamp B are coupled in a broadband RPSE system covering a wide spectral range $\Gamma = \Gamma_1 + \Gamma_2$, among which lamp A covering Γ_1 exhibits no residual polarization, and lamp B covering Γ_2 exhibits non-negligible residual polarization.

Here, we propose a so-called three-step method to calibrate the residual polarization in light source for a broadband RPSE system described above. In the proposed method, three related steps are performed in sequence to calibrate the parameters of RPSE system and

obtain b and c . **Step 1** is a global calibration over band Γ_1 with negligible residual polarization (absolute values of α' and β' are smaller than 5×10^{-3} generally) to get the rough systematic parameters of RPSE. The parameters include the initial azimuths of the analyzer and polarizer, the angle of incidence and the film thickness of the standard sample used in the calibration. Then **Step 2** is a wavelength-by-wavelength calibration in band Γ_2 with non-negligible dispersive residual polarization in light source to obtain residual polarization parameters b and c . In **Step 3**, with the residual polarization parameters b and c we again perform the global calibration but over the whole spectral range Γ to finally determine the systematic parameters, namely azimuths of the analyzer and polarizer, the angle of incidence, and the film thickness of the standard sample. Fig. 2 shows the whole performing process of the three-step calibration method. Details about the operations for each step of the method are given in the following.

Step 1. Global calibration is performed in band Γ_1 with negligible residual polarization (absolute values of α' and β' are smaller than 5×10^{-3}) to get rough values of systematic parameters.

Since the residual polarization in band Γ_1 is negligible, Eq. (2) is adopted. Multiple samples are measured to get the light intensity data. Then we perform Fourier analysis on the light intensity data in band Γ_1 to obtain the sequence of measured Fourier Dataset (\mathbf{MFD}_{Γ_1}). Theoretical Fourier Dataset (\mathbf{TFD}_{Γ_1}) is calculated by Eq. (4) and (5). In this calculation, an optical multilayer stacking model, involved the thickness d , angle of incidence AOI , the wavelength λ , and the refractive indices of samples, is constructed to describe the standard samples and calculate the theoretical ellipsometric angles ψ and Δ . Since the refractive indices of standard samples are well-known and stable optical constants, ψ and Δ are functions of d , AOI and λ . Hence, \mathbf{TFD}_{Γ_1} can be expressed as a function of the film thicknesses (d_1, d_2, \dots, d_m , where m is the number of standard samples), angle of incidence (AOI_1), initial azimuth angle of the polarizer (P_1), and the azimuth angle of the analyzer (A_1):

$$\mathbf{TFD}_{\Gamma_1} = f(d_1, d_2 \dots d_m, AOI_1, P_1, A_1). \quad (9)$$

When given the iterative initial values of the involved systematic parameters, the \mathbf{MFD}_{Γ_1} is fitted by the \mathbf{TFD}_{Γ_1} using a nonlinear regression iterative algorithm. Since all the involved parameters are non-dispersive, they are calibrated by a global iterative fitting. The mean squared error (MSE) is utilized to quantitate the difference between \mathbf{MFD}_{Γ_1} and \mathbf{TFD}_{Γ_1} , as defined by

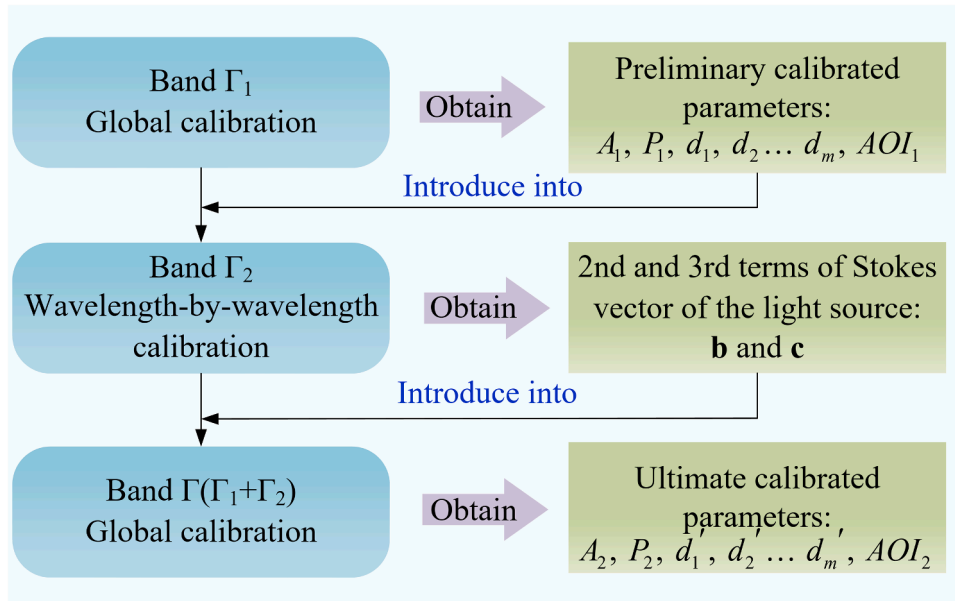


Fig. 2. Flowchart of three-step calibration method.

$$\begin{aligned}
MSE &= \frac{1}{\sqrt{2nm}} \left\{ \sum (MFD_{\Gamma_1} - TFD_{\Gamma_1})^2 \right\}^{1/2} \\
&= \frac{1}{\sqrt{2nm}} \left\{ \sum (\alpha_{mea} - \alpha_{theo})^2 + \sum (\beta_{mea} - \beta_{theo})^2 \right\}^{1/2},
\end{aligned} \tag{10}$$

where, n is the number of wavelengths in band Γ_1 , m is the number of samples, α_{mea} , β_{mea} and α_{theo} , β_{theo} are the measured and theoretical Fourier coefficient dataset respectively. Finally, one group of A_1 , P_1 , AOI_1 and thickness are obtained, which we consider close to the true value. However, in this step, the data of band Γ_2 is not considered, so it is not accurate enough.

Step 2. With systematic parameters roughly calibrated in step 1, wavelength-by-wavelength calibration is implemented in band Γ_2 with

$$\begin{aligned}
MSE &= \frac{1}{\sqrt{4nm}} \left\{ \sum (MFD_{\Gamma} - TFD_{\Gamma})^2 \right\}^{1/2} \\
&= \frac{1}{\sqrt{4nm}} \left\{ \sum (\alpha_{mea} - \alpha_{theo})^2 + \sum (\beta_{mea} - \beta_{theo})^2 + \sum (\alpha'_{mea} - \alpha'_{theo})^2 + \sum (\beta'_{mea} - \beta'_{theo})^2 \right\}^{1/2}.
\end{aligned} \tag{14}$$

non-negligible dispersive residual polarization in light source to obtain residual polarization parameters b and c .

Since the residual polarization in band Γ_2 cannot be neglected, quadruple frequency terms appear, and Eq. (3) is adopted to perform the Fourier analysis of intensity data in band Γ_2 of multiple samples to obtain the measured Fourier dataset MFD_{Γ_2} . Corresponding theoretical Fourier dataset TFD_{Γ_2} is calculated from the RPSE model for multiple standard film samples as given in Eq. (3). Fixing systematic parameters A_1 , P_1 , AOI_1 and thicknesses of standard samples (d_1, d_2, \dots, d_m) obtained in the step 1, TFD_{Γ_2} is functions only of residual polarization parameters b and c ,

$$TFD_{\Gamma_2} = f(b, c). \tag{11}$$

The iterative initial values of b and c for the first wavelength are given as 0, and the MFD_{Γ_2} is fitted by the TFD_{Γ_2} by a wavelength-by-wavelength nonlinear iterative algorithm since the residual polarization parameters b and c are dispersive. The output values b_1 and c_1 calibrated at the previous wavelength are used as the iterative initial values of b_{i+1} and c_{i+1} for the next wavelength. The MSE is utilized for the iterative calibration fitting,

$$\begin{aligned}
MSE_i &= \frac{1}{\sqrt{4m}} \left\{ (MFD_i - TFD_i)^2 \right\}^{1/2} \\
&= \frac{1}{\sqrt{4m}} \left\{ (\alpha_{mea} - \alpha_{theo})^2 + (\beta_{mea} - \beta_{theo})^2 + (\alpha'_{mea} - \alpha'_{theo})^2 + (\beta'_{mea} - \beta'_{theo})^2 \right\}^{1/2}, \\
&\quad i \in \Gamma_2
\end{aligned} \tag{12}$$

where, i is the i th wavelength point in band Γ_2 , MFD_i and TFD_i are respectively the measured and theoretical Fourier coefficients for the i th wavelength in Fourier datasets MFD_{Γ_2} and TFD_{Γ_2} . Finally, residual polarization parameters b and c in band Γ_2 are calibrated.

Step 3. Global calibration is performed in the whole band $\Gamma = \Gamma_1 + \Gamma_2$ to finally determine the systematic parameters with the residual polarization parameters b and c obtained in step 2.

Eq. (3) is adopted to perform Fourier analysis of the detected light intensity in the whole band Γ of multiple samples to get the measured Fourier dataset MFD_{Γ} . Theoretical Fourier dataset TFD_{Γ} can be calculated from the RPSE model as given in Eq. (3) for multiple standard samples. Since we can fix the residual polarization parameters b and c

using values obtained in step 2, the TFD_{Γ} is determined by thicknesses, angle of incidence, initial azimuth angle of the polarizer and the azimuth angle of the analyzer,

$$TFD_{\Gamma} = f(d'_1, d'_2, \dots, d'_m, AOI_2, P_2, A_2). \tag{13}$$

Herein, (d'_1, d'_2, \dots, d'_m) and A_2, P_2, AOI_2 represent film thicknesses of the standard samples, angle of incidence, initial azimuth angle of the polarizer and the azimuth angle of the analyzer in step 3, which are distinguished from those used for step 1. Output results of AOI_1, P_1, A_1 and (d_1, d_2, \dots, d_m) in step 1 are used as initial iterative values for step 3, and global calibration is implemented again by a nonlinear iterative algorithm to get the final systematic parameters. The evaluation function for step 3 is still the MSE as defined following,

3. Experimental set-up

Fig. 3 shows a diagram of RPSE 3D structure used as the experimental set-up in this paper. The light source consists of a halogen lamp (80017353, Heraeus), converging lens 1 (#45–872, Edmund Optics) and a deuterium lamp (DX277/05 J, Heraeus). The halogen lamp which can provide 400~1000 nm light, converges visible and near-infrared light to deuterium lamp through a converging lens 1. The deuterium lamp can provide 193~650 nm light. By deuterium-halogen composition, the light source covers an ultra-broadband of 193~1000 nm. The light emitted from the light source component is collimated by the collimating lens (#47–311, Edmund Optics), and then passes through the rotating polarizer which is a magnesium fluoride (MgF_2) Rochon polarizer (PUM2.08, B. Halle), and reaches the sample. The light reflected by the sample will pass through the fixed analyzer (PUM2.08, B. Halle), converging lens 2 (#84–280, Edmund Optics) successively and enter the spectrometer (Exemplar Plus, B&W TEK) in the end.

A set of mechanical structure has been designed to adjust the light path flexibly. All the lamps and lenses can move within limits to find the most suitable positions of focal points. The AOI can be adjusted conveniently by rotating two arms on the back disk where the dowel pins secure the equality between the angle of incidence and reflection. The adjustment range of AOI is from 20° to 90°

4. Results and discussion

We experimentally verified the correctness of three-step calibration method. Set the AOI of the RPSE to 60° , and turn on the deuterium and halogen lamps. Silica films on silicon substrates with nominal thickness of 20 nm, 66.5 nm and 100 nm are measured successively. Three systematic parameters, including A, P , the accurate value of AOI , as well as the accurate value of sample thickness, are all unknown and needed to be calibrated.

As mentioned in section 2.1, the presence of residual polarization in light source will cause the terms of quadruple frequency to appear in Eq. (3). Therefore, the values of Fourier coefficients α', β' could quantify the degree of residual polarization. We processed the light intensity data measured from 20 nm, 66.5 nm and 100 nm samples to get Hadamard data and then performed Fourier analysis to obtain the Fourier coefficients of quadruple frequency, which are shown in Fig. 4.

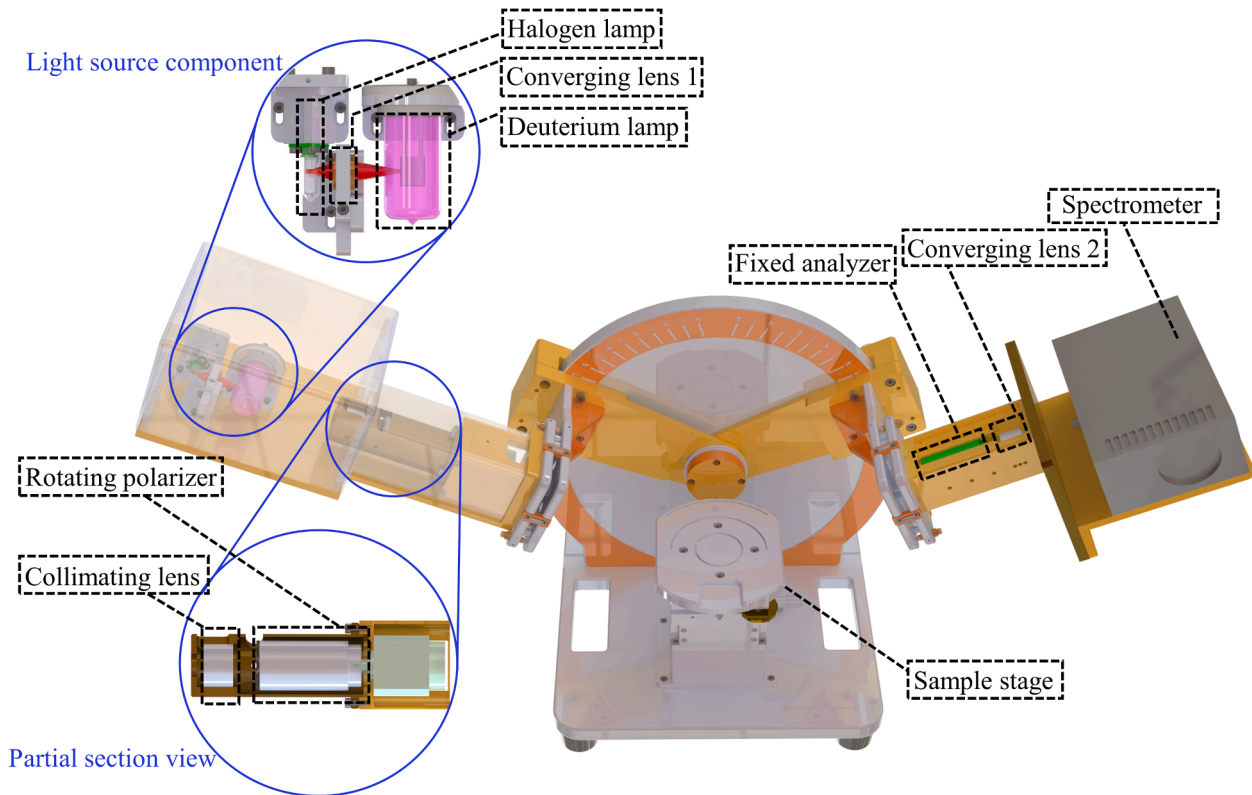


Fig. 3. Diagram of RPSE 3D structure.

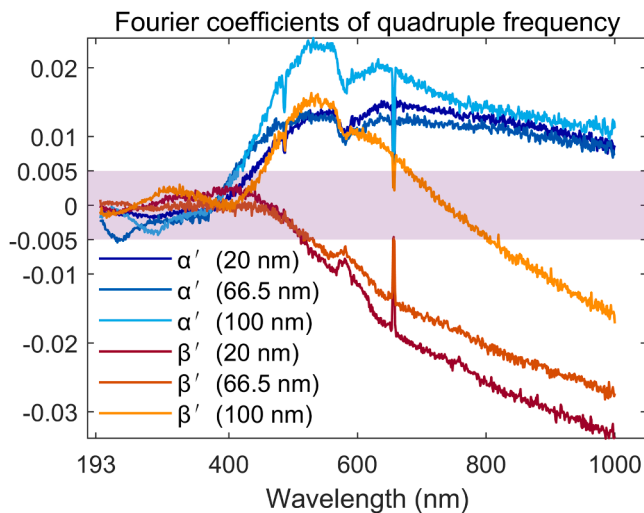


Fig. 4. Fourier coefficients of quadruple frequency for 20 nm, 66.5 nm and 100 nm SiO₂/Si samples. The data falling in the pink area is regarded as negligible.

It is clear from Fig. 4 that the terms of quadruple frequency do exist and show strong wavelength dependence. For wavelength less than 400 nm, the α' and β' for three samples are all between $\pm 5 \times 10^{-3}$ (area marked in pink) which can be basically ignored. But for wavelength more than 400 nm, the α' and β' rise sharply, reaching 0.02, a non-negligible magnitude.

The deuterium lamp has output from 193 nm to 650 nm around. We can see the characteristic peaks of the deuterium lamp at 486 nm and 656 nm in Fig. 4. The halogen lamp can cover 400~1000 nm, but has hardly any output in the wavelength less than 400 nm.

Thus, we can infer that without impacts of halogen lamp, there is no residual polarization in the range of 193~400 nm. However, the

situation in 400~1000 nm is more serious.

Assuming we ignore the α' and β' and directly use the α and β to calibrate system parameters of three samples respectively, the fitting curves are shown in Fig. 5. The calibration results are shown in Table 1.

It can be seen from Fig. 5 that the fitting is very poor by using only α and β . The measured data (blue and red dot lines) deviates from model (straight lines) a lot in some spectra. That's because some factors (b and c) are not involved in the calibration process, and it makes the system parameters we obtain are not accurate enough. The inaccurate system parameters could only guarantee some parts of spectrum a good fitting but not the whole spectrum.

Table 1 indicates that the MSE of three samples all are greater than 15. Calibration results of A , P and AOI for three samples all have differences about 1° . Hence, we couldn't determine the exact system parameters. Without the accurate system parameters, other samples can't be characterized. Thus, we adopt the three-step method with the consideration of residual polarization to calibrate the system. The calibration steps are as follows.

As shown in Fig. 4, the terms of quadruple frequency for wavelength less than 400 nm are very small. We believe that the values of b and c are 0 in 193~400 nm. In step 1, we use the light intensity of 193~400 nm band of three samples. Utilize only α and β , and perform global calibration of multiple samples. Two Fourier coefficient curves for one sample, a total of six Fourier coefficient curves to calibrate together. And then one set of A_1 , P_1 , d_1 , d_2 , d_3 and AOI_1 is obtained. The fitting curves are shown in Fig. 6 and calibration results are shown in Before correction row in Table 2. All three samples are fitted well in 193~400 nm and MSE (5.0595) is small.

In step 2, we calculate the Fourier coefficients of all double and quadruple frequency terms α , β , α' and β' of three samples in 400~1000 nm, and bring A_1 , P_1 , d_1 , d_2 , d_3 and AOI_1 to the system model and fix them. The values of b and c in 400~1000 nm are obtained wavelength by wavelength, as shown in Fig. 7. On the other hand, the b and c in 193~400 nm are 0. Accordingly, we get the full values of b and c in

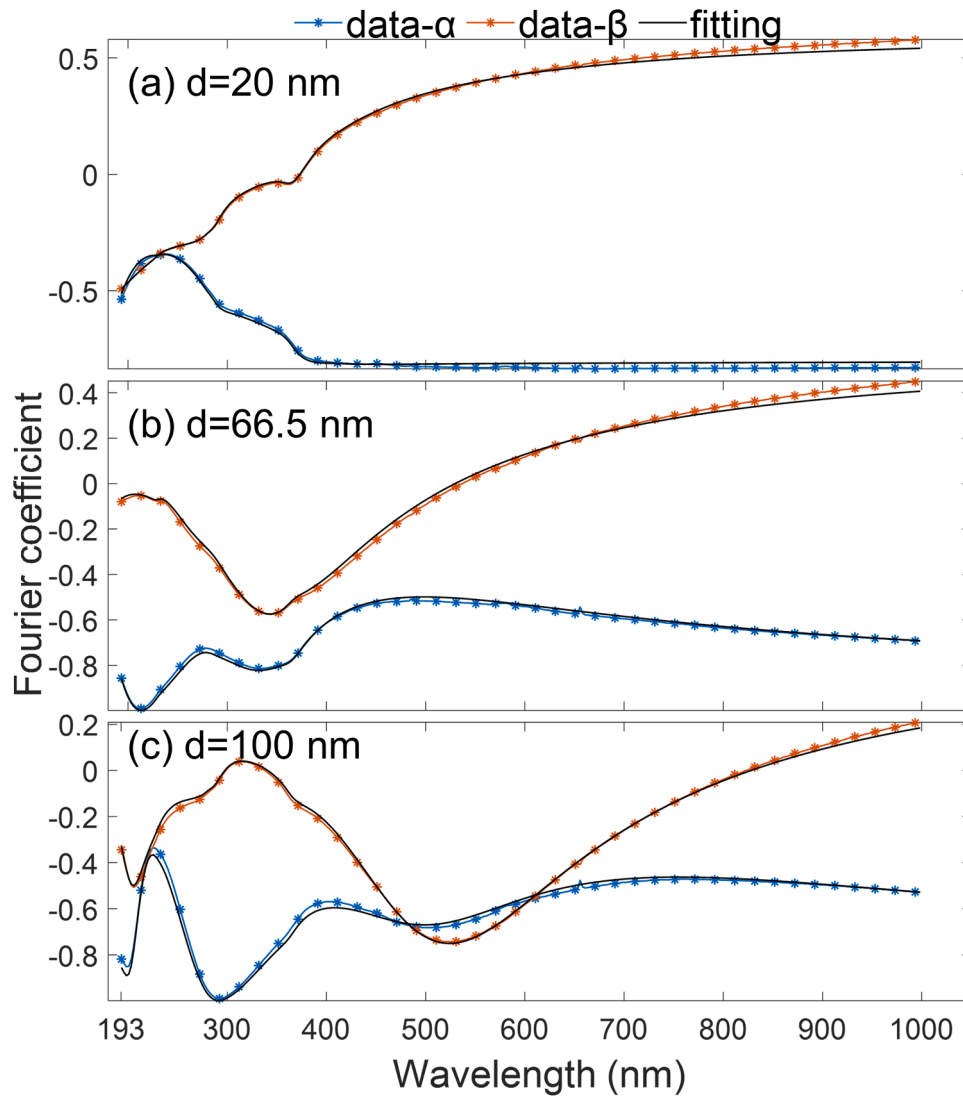


Fig. 5. Fitting curves of α and β for single sample (20 nm, 66.5 nm and 100 nm SiO₂/Si) calibration in 193~1000 nm without the residual polarization in light source considered.

Table 1
Single sample (20 nm, 66.5 nm and 100 nm SiO₂/Si) calibration results in 193~1000 nm.

Sample	Systematic parameters				
	A (°)	P (°)	d (nm)	AOI (°)	MSE
20 nm	31.10	-50.44	21.2	59.88	17.3917
66.5 nm	33.34	-48.11	65.6	58.99	16.3307
100 nm	32.13	-49.57	107.6	58.70	15.2667

193~1000 nm.

In the last step, we take the light intensity of three samples in 193~1000 nm and fix the b and c of the whole band in the system model as the known parameters. The α , β , α' , β' are used to calibrate globally to obtain the final parameters A_2 , P_2 , d_1' , d_2' , d_3' and AOI_2 which are shown in *After correction* in Table 2.

Fig. 8 illustrates the fitting curves and Table 2 shows the *After correction* results. The fitting performance in Fig. 8 is significantly improved compared with Fig. 5. The data fit the theoretical model almost perfectly. And the MSE of global calibration of multiple samples is only 4.4667. Hence it can be assumed that the parameters obtained from three-step calibration are accurate.

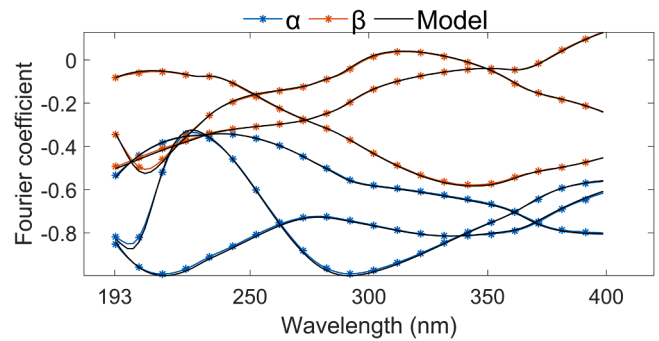


Fig. 6. Fitting curves of α and β in step 1 of the proposed three-step method for multiple samples (20 nm, 66.5 nm and 100 nm SiO₂/Si) calibration in 193~400 nm.

Then we measure another SiO₂ film of different thickness and make use of the ultimate calibration results (A_2 , P_2 , AOI_2) to calculate $N = \cos 2\psi$ and $C = \sin 2\psi \cos \Delta$ in Mueller matrix of the sample. Two sets of methods are used to obtain N and C . In the first method, Eq. (2) is adopted to calculate N and C which are shown in Fig. 9 and labeled as

Table 2

Comparison of calibrated systematic parameters of the broadband RPSE before and after correcting the residual polarization in light source.

Before correction	A_1 (°)	P_1 (°)	d_1 (nm)	d_2 (nm)	d_3 (nm)	AOI_1 (°)	MSE
	31.49	-49.73	21.8	66.2	108.5	59.81	5.0595
After correction	A_2 (°)	P_2 (°)	d_1' (nm)	d_2' (nm)	d_3' (nm)	AOI_2 (°)	MSE
	31.21	-50.16	22.0	65.7	108.6	59.82	4.4667

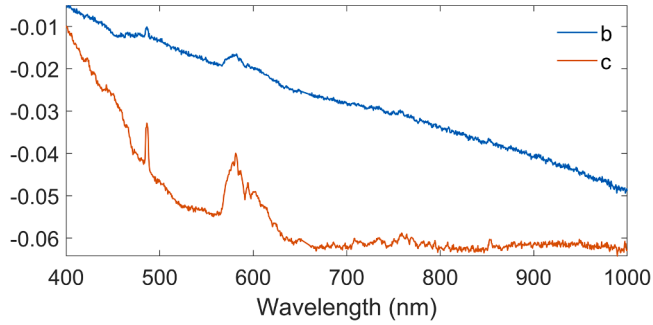


Fig. 7. Calibration results of b and c in step 2 of the proposed three-step method in 400~1000 nm.

before correction. And in the second method, Eqs (3)-(8) and parameters b and c are adopted to calculate N and C which are also shown in Fig. 9 and labeled as *after correction*. Fig. 9 demonstrates that three-step method could modify our calculation results ($MSE=3.84$) greatly compared with the common method without any correction ($MSE=15.76$).

Apart from SiO_2 film, other materials have also been tested to further demonstrate the accuracy improvement by correcting the residual polarization using our proposed method. Fig. 10 comparatively shows the measured ellipsometric spectra $N = \cos 2\psi$ and $C = \sin 2\psi \cos \Delta$ of the Au/ SiO_2 / Si film before and after correction of the residual polarization as well as the best fitting results. The thicknesses of the Au layer and the SiO_2 layer are 27.9 nm and 101 nm, respectively. It can be seen that the corrected spectra fit the theoretical results much better than the uncorrected ones, indicating the measurement accuracy improve significantly after calibrating and correcting the residual polarization in the light source by using our proposed methods.

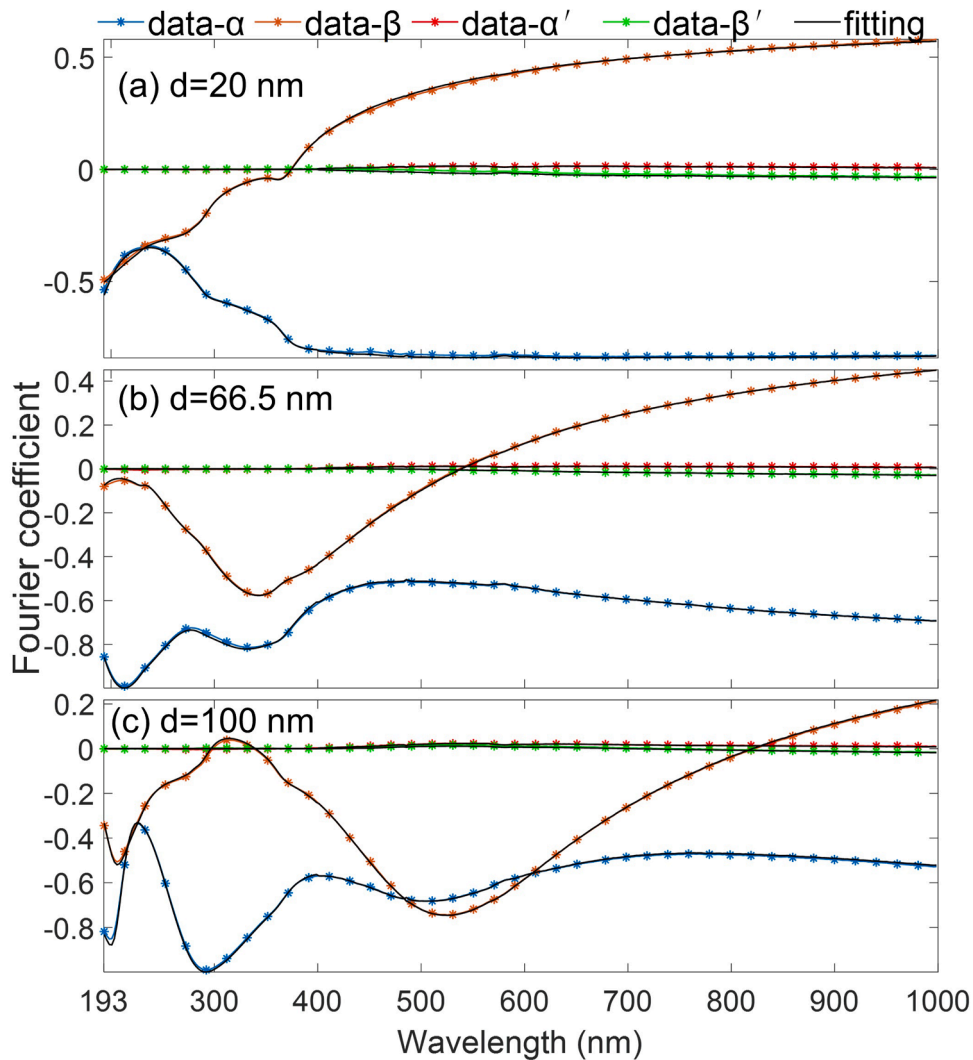


Fig. 8. Fitting curves of α , β , α' and β' in step 3 of the proposed three-step method for multiple samples (20 nm, 66.5 nm and 100 nm SiO_2/Si) calibration in 193~1000 nm with the residual polarization in light source considered.

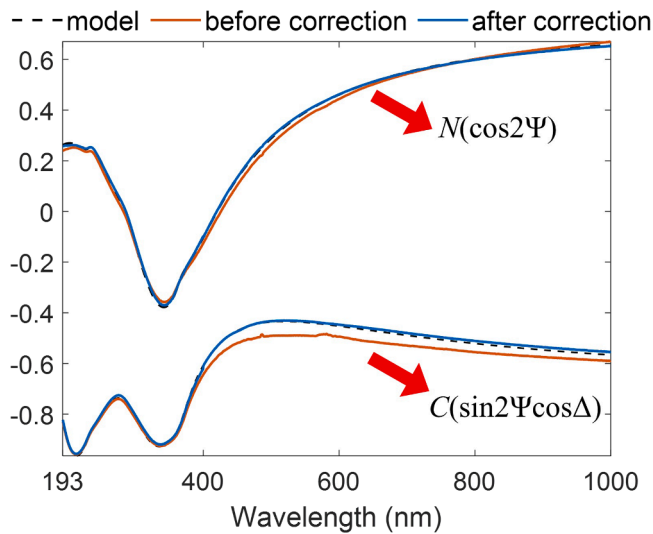


Fig. 9. Comparison of calculation results (N and C) of SiO_2 film before and after correction.

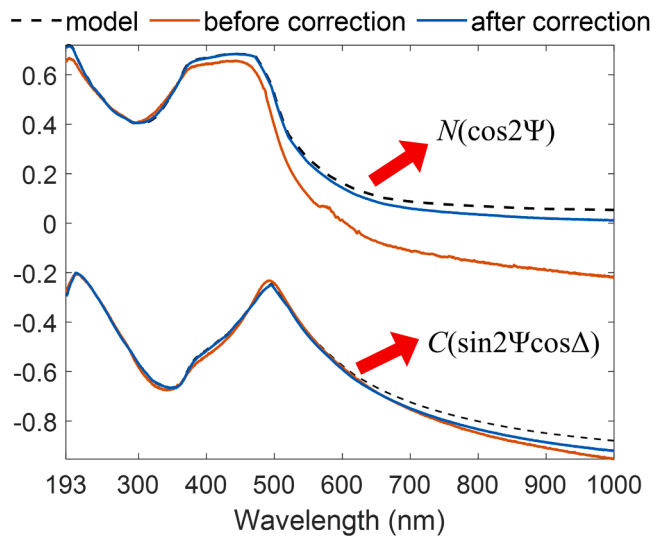


Fig. 10. Experimental ellipsometric spectra (N and C) of $\text{Au/SiO}_2/\text{Si}$ film before and after correction and the best fitting results.

5. Conclusion

In summary, a method is proposed to solve the impact of residual polarization in light source on calibration and measurement without changing the RPSE structure. Firstly, the source of error is figured out by mathematical derivation of system model for RPSE. We find that due to the light of partial polarization, the small quantity of the second and third terms in the Stokes vector of light emitted from the light source could cause quadruple frequency terms to appear in the irradiance expression the detector receives, thus bias the calibration and measurement results. Consequently, we propose a comprehensive three-step method to calibrate and correct residual polarization and verify it with homemade RPSE instrument. In this three-step method, by taking advantage of the deuterium lamp in 193–400 nm, and through two global calibrations and one wavelength by wavelength calibration, the measured Fourier coefficients fit perfectly with the model and the wavelength dependent values of b and c in Stokes vector of the light source are obtained, as well as the systemic parameters. As long as a rotating polarizer is attached directly after a light source which has

residual polarization, the problem would occur. Therefore, our three-step calibration can also be promoted to other broadband ellipsometry system, which is instructive for ellipsometry calibration.

CRediT authorship contribution statement

Ming Gong: Methodology, Formal analysis, Investigation, Writing – original draft. **Honggang Gu:** Conceptualization, Methodology, Writing – review & editing, Supervision, Project administration, Funding acquisition. **Chao Chen:** Validation, Formal analysis, Writing – review & editing. **Jun Chen:** Validation, Writing – review & editing. **Weiqi Li:** Validation, Writing – review & editing. **Chuanwei Zhang:** Validation, Writing – review & editing, Supervision. **Shiyuan Liu:** Writing – review & editing, Supervision, Project administration, Funding acquisition.

Declaration of Competing Interest

The authors declare that they have no known competing financial interests or personal relationships that could have appeared to influence the work reported in this paper.

Data availability

Data will be made available on request.

Acknowledgments

The authors also thank the technical support from the Experiment centre for Advanced Manufacturing and Technology in School of Mechanical Science & Engineering of HUST.

Funding

This work was supported by the National Natural Science Foundation of China [52130504, 51727809], Key Research and Development Plan of Hubei Province [2021BAA013], Natural Science Foundation of Hubei Province [2021CFB322], and the Fundamental Research Funds for the Central Universities [2021XXJ113].

Reference

- [1] S. Liu, X. Chen, C. Zhang, Development of a broadband Mueller matrix ellipsometer as a powerful tool for nanostructure metrology, *Thin Solid Films* 584 (2015) 176–185.
- [2] H. Gu, H. Jiang, X. Chen, C. Zhang, S. Liu, Superachromatic polarization modulator for stable and complete polarization measurement over an ultra-wide spectral range, *Opt. Express* 30 (9) (2022) 15113–15133.
- [3] R.M.A. Azzam and N.M. Bashara, *Ellipsometry and Polarized Light*. (Amsterdam, 1977).
- [4] H.G. Tompkins, E.A. Irene, *Handbook of Ellipsometry*, Springer, 2005.
- [5] H. Fujiwara, *Spectroscopic Ellipsometry: Principles and Applications*, Wiley, 2007.
- [6] M. Losurdo, K. Hingerl, *Ellipsometry At the Nanoscale*, Springer, 2013.
- [7] R.M.A. Azzam, Stokes-vector and Mueller-matrix polarimetry [Invited], *J. Opt. Soc. Am. A* 33 (7) (2016) 1396–1408.
- [8] J. Hough, Polarimetry: a powerful diagnostic tool in astronomy, *Astron. Geophys.* 47 (3) (2006) 3.31–3.35.
- [9] M. Losurdo, M. Bergmair, G. Bruno, D. Cattelan, C. Cobet, A. de Martino, K. Fleischer, Z. Dohcevic-Mitrovic, N. Esser, M. Galliet, R. Gajic, D. Hemzal, K. Hingerl, J. Humlicek, R. Ossikovski, Z.V. Popovic, O. Saxl, Spectroscopic ellipsometry and polarimetry for materials and systems analysis at the nanometer scale: state-of-the-art, potential, and perspectives, *J. Nanopart. Res.* 11 (2009) 1521–1554.
- [10] R.M.A. Azzam, A simple Fourier photopolarimeter with rotating polarizer and analyzer for measuring Jones and Mueller matrices, *Opt. Commun.* 25 (2) (1978) 137–140.
- [11] J.M. Bueno, Polarimetry using liquid-crystal variable retarders: theory and calibration, *J. Opt. A: Pure Appl. Opt.* 2 (3) (2000) 216–222.
- [12] R.M.A. Azzam, Division-of-amplitude photopolarimeter (DOAP) for the simultaneous measurement of all four Stokes parameters of light, *Opt. Acta* 29 (5) (1982) 685–689.
- [13] D.E. Aspnes, Expanding horizons: new developments in ellipsometry and polarimetry, *Thin Solid Films* (2004) 455–456, 3-13.

- [14] D.E. Aspnes, Spectroscopic ellipsometry – Past, present, and future, *Thin Solid Films* 571 (2014) 334–344.
- [15] H. Gu, X. Chen, H. Jiang, C. Zhang, S. Liu, Optimal broadband Mueller matrix ellipsometer using multi-waveplates with flexibly oriented axes, *J. Opt.* 18 (2) (2016), 025702.
- [16] L. Broch, A. En. Naciri, L. Johann, Systematic errors for a Mueller matrix dual rotating compensator ellipsometer, *Opt. Express* 16 (12) (2008) 8814–8824.
- [17] J. Li, B. Ramanujam, R.W. Collins, Dual rotating compensator ellipsometry: theory and simulations, *Thin Solid Films* 519 (9) (2011) 2725–2729.
- [18] X. Chen, C. Zhang, S. Liu, Depolarization effects from nanoimprinted grating structures as measured by Mueller matrix polarimetry, *Appl. Phys. Lett.* 103 (15) (2013), 151605.
- [19] Z. Guo, H. Gu, M. Fang, L. Ye, S. Liu, Giant in-plane optical and electronic anisotropy in tellurene: a quantitative exploration, *Nanoscale* 14 (2022) 12238–12246.
- [20] Z. Guo, H. Gu, M. Fang, B. Song, W. Wang, X. Chen, C. Zhang, H. Jiang, L. Wang, S. Liu, Complete dielectric tensor and giant optical anisotropy in quasi-one-dimensional ZrTe₅, *ACS Mater. Lett.* 3 (2021) 525–534.
- [21] E. Garcia-Caurel, A. De Martino, J.P. Gaston, L. Yan, Application of Spectroscopic Ellipsometry and Mueller Ellipsometry to Optical Characterization, *Appl. Spectrosc.* 67 (1) (2013) 1–21.
- [22] N.V. Nguyen, B.S. Pudliner, I. An, R.W. Collins, Error correction for calibration and data reduction in rotating-polarizer ellipsometry: applications to a novel multichannel ellipsometer, *J. Opt. Soc. Am. A* 8 (6) (1991) 919–931.
- [23] A. Straaijer, M.H.W. Verbruggen, J.M.M. de Nijs, H.H. Brongersma, Novel fast spectroscopic rotating-polarizer ellipsometer, *Rev. Sci. Instrum.* 64 (1993) 1468.
- [24] A.En Naciri, L. Broch, L. Johann, R. Kleim, Fixed polarizer, rotating-polarizer and fixed analyzer spectroscopic ellipsometer: accurate calibration method, effect of errors and testing, *Thin Solid Films* 406 (1–2) (2002) 103–112.
- [25] A.R.M. Zaghoul, R.M.A. Azzam, Single-element rotating-polarizer ellipsometer: PSI meter, *Surf. Sci* 96 (1–3) (1980) 168–173.
- [26] S.H. Russev, Correction for nonlinearity and polarization-dependent sensitivity in the detection system of rotating analyzer ellipsometers, *Appl. Opt.* 28 (8) (1989) 1504–1507.
- [27] S. Park, D. Gweon, Optimal calibration for rotating analyzer ellipsometer, *J. Mech. Sci. Technol* 19 (11) (2005) 2165–2171.
- [28] A. Herawati, R.A.N. Khasanah, L.Z. Maulana, E. Suharyadi, I. Santoso, Simple and Low-Cost Rotating Analyzer Ellipsometer (RAE) for Wavelength Dependent Optical Constant Characterization of Novel Materials, *Key Eng. Mater.* 840 (2020) 392–398.
- [29] I.K.A.P. Dana, P.D. Jatmiko, E. Suharyadi, I. Santoso, A compact, modular, multi-wavelength (200–850nm) rotating-analyzer ellipsometer for optical constant characterization of nanostructured materials, *Eur. J. Phys* 41 (6) (2020) 65303.
- [30] S. Kawabata, M. Motoki, H. Yokota, Calibration method of the specific characteristic of an electronic system of a rotating-analyzer ellipsometer, *Appl. Opt.* 36 (10) (1997) 2178–2182.
- [31] R.M.A. Azzam, N.M. Bashara, Analysis of systematic errors in rotating-analyzer ellipsometers, *J. Opt. Soc. Am.* 64 (11) (1974) 1495, 1469.
- [32] T.M. El-Agez, A.A. El Tayyan, S.A. Taya, Rotating polarizer-analyzer scanning ellipsometer, *Thin Solid Films* 518 (19) (2010) 5610–5614.
- [33] S.A. Taya, T.M. El-Agez, A.A. Alkanoo, A spectroscopic ellipsometer using rotating polarizer and analyzer at a speed ratio 1:1 and a compensator, *Opt Quantum Electron* 46 (2014) 883–895.
- [34] T.M. El-Agez, S.A. Taya, Development and construction of rotating polarizer analyzer ellipsometer, *Opt Lasers Eng* 49 (4) (2011) 507–513.
- [35] L.Y. Chen, D.W. Lynch, Scanning ellipsometer by rotating polarizer and analyzer, *Appl. Opt.* 26 (24) (1987) 5221–5228.
- [36] H. Tu, Y. Zheng, Y. Shan, Y. Chen, H. Zhang, R. Zhang, S. Wang, J. Li, Y. Lee, L. Chen, Method for Analyzing the Measurement Error with Respect to Azimuth and Incident Angle for the Rotating Polarizer Analyzer Ellipsometer, *Crystals* 11 (4) (2021) 349.
- [37] G. Xia, R. Zhang, Y. Chen, H. Zhao, S. Wang, S. Zhou, Y. Zheng, Y. Yang, L. Chen, New design of the variable angle infrared spectroscopic ellipsometer using double Fourier transforms, *Rev. Sci. Instrum.* 71 (7) (2000) 2677–2683.
- [38] S. Bertucci, A. Pawlowski, N. Nicolas, L. Johann, A. El Ghemmaz, N. Stein, R. Kleim, Systematic errors in fixed polarizer, rotating polarizer, sample, fixed analyzer spectroscopic ellipsometry, *Thin Solid Films* 313–314 (13) (1998) 73–78.
- [39] N.J. Diorio Jr, M.R. Fisch, J.L. West, Filled liquid crystal depolarizers, *J. Appl. Phys* 90 (8) (2001) 3675–3678.
- [40] Y. Wang, W. Zhu, C. Zhang, Q. Fan, L. Chen, H. Lezec, A. Agrawal, T. Xu, Ultra-compact visible light depolarizer based on dielectric metasurface, *Appl. Phys. Lett.* 116 (5) (2020) 0511031–0511035.